

Development of an Electrical Phantom for Multi-Frequency Electrical Impedance Tomography based on the Visible Human Project

T. Menden¹, J. Orschulik¹, M. Slimi¹, S. Leonhardt¹, M. Walter¹

¹Chair for Medical Information Technology, RWTH Aachen University, Pauwelsstr. 20, Aachen, Germany
Contact: menden@hia.rwth-aachen.de

Introduction

Electrical Impedance Tomography (EIT) is a biomedical imaging modality to monitor regional changes of conductivity distribution inside the human body. Therefore, a small alternating current is injected inside the body and the resulting surface potential is measured. EIT is mainly used to monitor mechanical ventilation, lung perfusion and pulmonary function testing [1]. Many different research EIT-devices have been developed for these purposes. Before applying them to living organisms, the performance of such systems has to be evaluated with test measurements at EIT-phantoms. In general, test units can be classified into two main types: physical- and electrical-phantoms. Typically, a physical phantom tries to mimic the human body utilizing a tank filled with a conductive fluid and volume elements similar to organs of the body [2, 3]. The device under test can be connected directly to the phantom without the disturbance of unknown electrode-impedances. The drawback of conductive fluids is a temporal drift due to changes of ionic concentrations, temperature and volume. Additionally, most of the conductive fluids have a poor capacitive behavior. The second class of EIT-phantoms are electrical dummies. Biological tissue has a resistive- and capacitive-component, which can be modeled as a combination of passive R- and C-elements as described by Cole [4]. A whole RC-network creates an electrical phantom. In general, phantoms could also include active components. The great advantage of these electrical systems is the reproducibility and accuracy. The downside, compared to the biological phantoms, is the lack of authenticity, due to the finite number of discrete electrical elements.

In this paper, we propose a method to convert a finite-element model of the thorax with typical tissue conductivities into an electrical circuit with 32 electrodes. The developed circuit of the dummy includes frequency depended components of the tissue. Simulated EIT-measurements of the new developed dummy are compared to the forward solution of the original model to evaluate the performance of the electrical approximation.

Materials and Methods

The human body can be treated as a volume conductor composed of an infinite number of conducting elements. For a sufficiently small element size and large element number, the body can be approximated accurately as a finite element mesh (FEM). The edges of the model can be transformed into an electrical circuit, as described later. The crucial question is: How can the amount of elements be

reduced with a minimum of accuracy loss, so that the phantom is physically manufacturable. We developed a method to map a 3D-thorax model to a 2D-shaped electrical circuit in the frequency range between 50kHz to 1MHz. Therefore, the solution is optimized that the resulting measurement voltages match the original high resolution model.

Modeling of the Thorax

This work is based on the thorax model of Grychtol et al. [5], which is constructed out of data of the Visible Human Project [6]. All simulation and calculations were performed in Matlab using EIDORS [7]. The model was created with 32 electrodes aligned in a single plane between the 6th and 7th intercostal space. This results in a finite element mesh of 53570 nodes and 259784 elements and is shown in fig. 1.

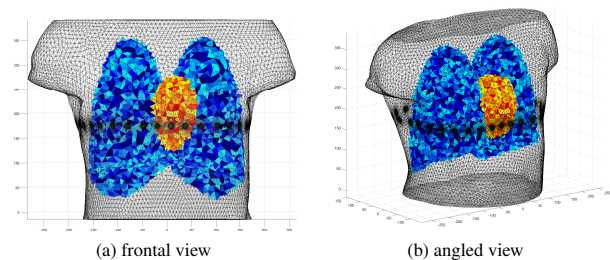


Figure 1: 3D-finite element mesh used to generate the required surface voltages for the EIT-Phantom.

The conductivities of right- and left-lung, as well as heart and background, can be set independently. The complex conductivity is given by

$$\underline{\sigma}(j\omega) = \sigma(\omega) + j\omega\varepsilon_0\varepsilon_r(\omega), \quad (1)$$

where σ is the conductivity, ε_r is the permittivity, specific for each tissue at the given frequency ω . ε_0 is defined as the vacuum permittivity. In this paper the conductivity was derived from the IFAC-Project [8] based on the publication of Gabriel [9]. The tissues "LungInspiration", "Heart" and "Muscle" were implemented at four different frequencies ω_k (50kHz, 100kHz, 250kHz and 500kHz), which are in the β -dispersion range and typical for EIT measurements. The Cole-model approximates the complex specific impedance of tissue $\underline{\rho}(j\omega)$ with the circuit in fig. 2 and eq. 2:

$$\underline{\rho}(j\omega) = \rho_\infty + \frac{\rho_0 - \rho_\infty}{1 + j\omega\tau}, \quad \{\rho_\infty, \rho_0, \tau\} > 0 \wedge \rho_0 > \rho_\infty, \quad (2)$$

where ρ_0 is the specific tissue impedance at 0Hz, ρ_∞ at ∞ Hz and $\tau = (\rho_0 - \rho_\infty)C$.

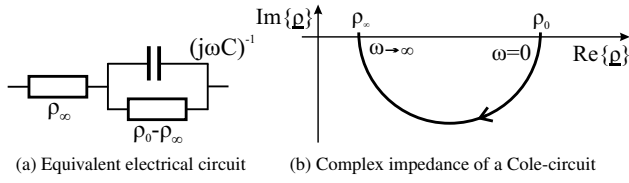


Figure 2: Electrical circuit that corresponds to the tissue behavior in the β -dispersion from Cole [4].

2D Projection

We use a 2D-finite element mesh with 1024 elements as the final phantom structure. Due to the small amount of elements and the 2D-shape, the resulting phantom is physically manufacturable. The 2D-model, depicted in fig. 3, is shaped similarly to a slice of the 3D-model. The forward

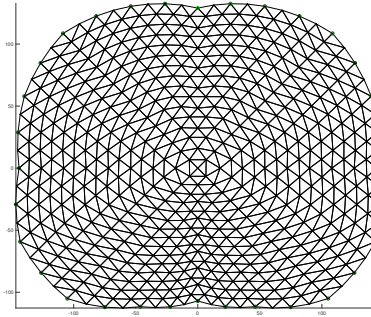


Figure 3: 2D-finite element mesh for the EIT-Phantom. Each element was optimized to match the 3D-forward voltages. Finally, each edge was transformed into electrical components.

problem in EIT describes the calculation of the measured surface voltages as a result of the injected current in the volume conductor with a given conductivity distribution. The described model above results in 928 voltage measurements \vec{v}_{3D} for a skip-4 pattern. The voltage measurements \vec{v}_{2D} of the 2D-model are given by the nonlinear function $\vec{f}_{2D}(\vec{\sigma})$ for a conductivity distribution

$$\underline{\sigma}_i = \frac{1}{\underline{\rho}_i} = \frac{1 + j\omega\tau_i}{\rho_{0i} + j\omega\tau\rho_{\infty i}} \quad (3)$$

of the 2D-model with $i = 1024$ elements. The minimization function

$$\min_{\vec{\sigma}} \|\vec{f}_{2D}(\vec{\sigma}) - \vec{v}_{3D}\|_2^2, \quad (4)$$

describes the optimization problem of the 2D-model for the complex conductivity distribution $\vec{\sigma}$ with the smallest difference between \vec{v}_{3D} and \vec{v}_{2D} . Due to the complex value of $\vec{v}_{2D,3D}$, the real and imaginary component of the minimization function was normalized to reduce the influence of small absolute voltage differences:

$$\min_{\vec{\sigma}} \left\| \frac{\Re\{\vec{f}(\vec{\sigma}) - \vec{v}\}}{\Re\{\vec{v}\}} \right\|_2^2 + \left\| \frac{\Im\{\vec{f}(\vec{\sigma}) - \vec{v}\}}{\Im\{\vec{v}\}} \right\|_2^2, \quad (5)$$

where $\vec{v} = \vec{v}_{3D}$. In order to address the multifrequent component of the phantom, the specific frequency ω_k of each 3D-model is added to the minimization term:

$$\min_{\vec{\sigma}} \sum_{k=1}^m \left\| \frac{\Re\{\vec{f}(\vec{\sigma}, \omega_k) - \vec{v}(\omega_k)\}}{\Re\{\vec{v}(\omega_k)\}} \right\|_2^2 + \left\| \frac{\Im\{\vec{f}(\vec{\sigma}, \omega_k) - \vec{v}(\omega_k)\}}{\Im\{\vec{v}(\omega_k)\}} \right\|_2^2 + \mathbf{R} \quad (6)$$

In addition, q_e is extended with a regularization term to reduce huge variations between neighboring elements, which do not occur in reality. \mathbf{R} is given as:

$$\mathbf{R} = \lambda_r \cdot \|L \cdot \Re\{\vec{\sigma}(\omega_k)\}\|_2^2 + \lambda_i \cdot \|L \cdot \Im\{\vec{\sigma}(\omega_k)\}\|_2^2, \quad (7)$$

where L is the regularization prior matrix, to create a smoother conductivity distribution. $\lambda_{r,i}$ is the regularization parameter, which is set empirically and defines the impact of the regularization. The complex conductivity distribution $\vec{\sigma} = \frac{1}{\underline{\rho}}$ underlies the boundary conditions given in eq. 2. These boundary conditions assure that the solution of the minimization function is physically realizable. The minimization problem is solved combining the Trust-Region-Reflective algorithm with the Levenberg-Marquardt algorithm [10].

Approximation of Cole-Parameters

The previous section presented a method to generate a 2D-finite element mesh with complex conductivity values $\underline{\sigma}$ for each triangle. Gagnon et al. [11] describes the relationship of a conductiv triangle element to the admittance of an edge as depicted in fig. 4. Ohm's law, $\mathbf{Y} \cdot \mathbf{V} = \mathbf{I}$ describes

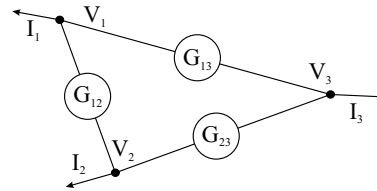


Figure 4: Minimalistic mesh with three nodes and three admittances that represent one triangle element with constant conductivity.

the relation of the voltage vector $\mathbf{V} = [V_1, V_2, V_3]^T$ and the current vector $\mathbf{I} = [I_1, I_2, I_3]^T$ through the admittance matrix \mathbf{Y} . This matrix is composed of the admittances G_{12} , G_{13} and G_{23} and is derived from Kirchhoff's current law.

These admittances are directly related to $\underline{\sigma}$ and the relative position of the nodes to each other. \mathbf{Y} is the system matrix of the 2D-mesh with the conductivity $\vec{\sigma}$. Therefore, the Cole-parameter (ρ_{∞}, ρ_0 and τ) of the conductivity distribution $\vec{\sigma}$ were transformed into complex admittances $\mathbf{Y}(\omega_k)$ for each frequency. Each element corresponds to an edge of the 2D-mesh. The inversion of \mathbf{Y} leads to the impedance matrix

$$\mathbf{Z}(\omega_k) = \mathbf{Y}(\omega_k)^{-1}. \quad (8)$$

Due to the assumption in eq. 2, each element of $\mathbf{Z}(\omega_k)$ should be a Cole-circuit and describe a semicircle in the 4th quadrant. The impedance can be described as:

$$\mathbf{Z}(\omega) = R_\infty + \frac{R_0 - R_\infty}{1 + j\omega C \cdot (R_0 - R_\infty)}, \quad (9)$$

where R_∞ , R_0 and C are the final components of each edge of the mesh and described with ξ . Therefore, the impedance values of each edge were fitted to the parameter of eq. 9 for the four investigated frequencies. The resulting minimization problem is:

$$\min_{\xi} \sum_{k=1}^m \left\| \frac{\text{Re}\{\vec{\mathbf{Z}}(\xi, \omega_k) - \mathbf{Z}(\omega_k)\}}{\text{Re}\{\mathbf{Z}(\omega_k)\}} \right\|_2^2 + \left\| \frac{\text{Im}\{\vec{\mathbf{Z}}(\xi, \omega_k) - \mathbf{Z}(\omega_k)\}}{\text{Im}\{\mathbf{Z}(\omega_k)\}} \right\|_2^2, \quad (10)$$

where $\vec{\mathbf{Z}}(\omega_k)$ is the impedance of each edge of the mesh resulting out of the component parameters ξ . The problem is solved with the Trust-Region-Reflective algorithm with "multistart" option.

Results and Discussion

2D Projection

The minimization function given in eq. converges and results in a distribution with (ρ_∞, ρ_0) and τ for each element. The resulting conductivity distribution is calculated for each frequency and is shown exemplary for 50kHz in fig. 5. The forward solution of these distributions were cal-

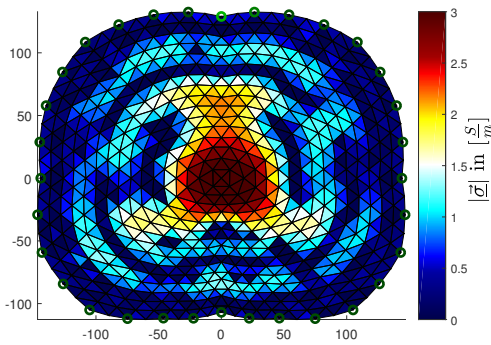


Figure 5: Each element of the 2D-mesh gives the absolute conductivity at 50kHz as a result of the optimization process.

culated and compared with the values of the thorax model from the beginning. The relative measurement error compared of each frequency is shown in tab. 1.

Approximation of Cole-Parameters

Each edge of the 2D-mesh ξ was transformed into electrical circuits. This optimization step results partially in $\rho_0 < \rho_\infty$ which does not correlate with the traditional

Table 1: Relative error of the resulting forward voltages after 2D projection.

$\delta_U \cdot 100\%$	50kHz	100kHz	250kHz	500kHz
real	1.98	1.84	2.19	2.40
imag	0.29	0.78	1.47	1.23

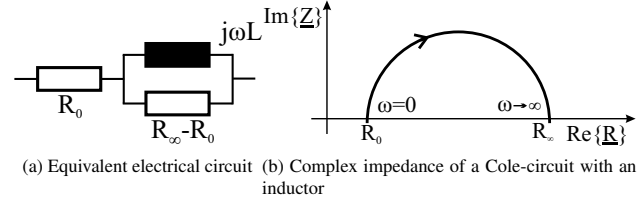


Figure 6: Electrical circuit that corresponds to the behavior of some resulting elements with a positive imaginary component.

Cole-model. Therefore, the model of fig. 6 was used for these elements.

The relation of ρ_0 and ρ_∞ is switched due to the usage of an inductor instead of the capacitor. Hence, the Cole curve is mirrored in the first quadrant and meet the optimization result. 96.6 % of the $n = 1568$ edges could be realized with the traditional Cole equivalent circuit.

The remaining 53 elements were inductor-based and located in boundary regions. To evaluate the quality of the component calculation, the relative error

$$\delta_{Z_i} = \left| \frac{Z_{opt_i} - Z_i(\omega_k)}{Z_i(\omega_k)} \right|, \quad (11)$$

$$\delta_Z = \frac{\sum_{i=1}^n \delta_{Z_i}}{n} \quad (12)$$

was calculated, where $Z_i(\omega_k)$ is the impedance of the 2D-mesh before the optimization and Z_{opt_i} after the optimization of a single element. The relative error δ_Z is listed for each frequency in tab. 2.

Table 2: Relative error of the transformation from the conductivity of FEM-elements to equivalent component impedances of the edges.

$\delta_Z \cdot 100\%$	50kHz	100kHz	250kHz	500kHz
real	3.01	2.86	2.84	3.09
imag	2.46	1.76	1.70	2.13

Discussion

Each of the two transformation processes reduces the accuracy of the resulting EIT-phantom. The final performance of the new developed phantom is evaluated with a Simulink testbench, which emulates a skip-4 EIT measurement and calculates the resulting voltages \vec{v}_{sim} , called u-shapes. These u-shapes are compared with the forward solution of the original 3D-thorax model \vec{v}_{3D} , shown in

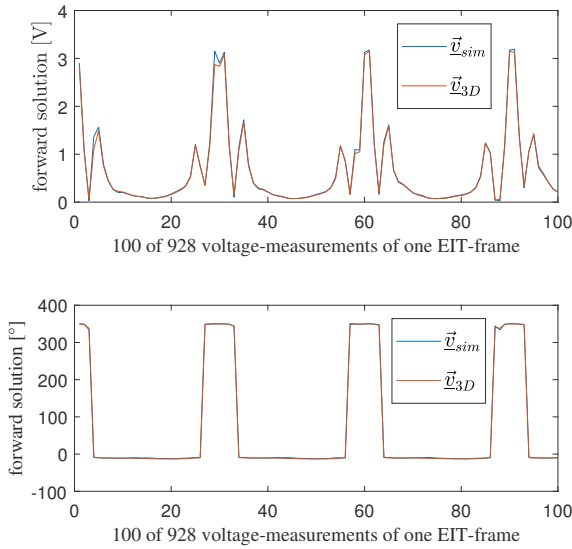


Figure 7: Voltages of the simulated dummy compared to the surface voltages of the 3D-FEM model at 50 kHz.

fig. 7. Consequently, the relative error δ_{sim} between \vec{v}_{sim} and \vec{v}_{3D} is calculated for each desired frequency and shown in tab. 3. The overall error, between the measured volt-

Table 3: Relative error of the transformation from the conductivity of FEM-elements to equivalent component impedances of the edges.

$\delta_{sim} \cdot 100\%$	50kHz	100kHz	250kHz	500kHz
real	8.77	8.69	8.74	9.04
imag	9.51	7.77	8.08	12.01

ages is for most of the inspected frequencies under 10%. The voltage difference between 50kHz and 500kHz of the original thorax model is approximately 30%. The measurement error occurring through the model reduction approach is about factor three smaller. We assume, that the error is small enough to ensure a noticeable difference in the declared frequency range.

Another interesting aspect is the usage of inductors for a pure capacitive model. A negative imaginary component occurs in the boundary region, due to the second optimization process. This is a result of the Trust-Region Reflective solver. We assume, that this is also a valid solution, even though it is not a physiological representation.

A further validation of the phantom is necessary to ensure a sufficient accuracy and valid reconstruction results.

Conclusions and Outlook

We developed a method to transform a 3D-FEM model with 259784 elements of a male thorax into a 2D-electrical circuit for EIT-measurements on a phantom using 1024 elements. Most of the proposed approaches in literature try to convert conductivities of a FEM-model directly into electrical components. This always has the drawback of accuracy

loss, due to the finite quantity of components. We suggest to fit the electrical components of the dummy so that the resulting surface voltages of an EIT measurement mimic the behavior of the high resolution model. Therefore, we propose a two-step optimization procedure to first, reduce the 3D-model to a 2D-model and keep the measured voltages equivalently. This results in a measurement error of maximum 2.4% for four inspected frequencies. In a second step, the edges of the 2D-model are transferred to electrical components of a Cole-model. The maximum error of this transformation is below 3.09%. The final model contains 3242 resistors, 1515 capacitors and 53 inductors.

The described phantom is optimized in four frequency points which could be extended in the future to cover a wider spectrum and smaller frequency step size. In the future, we will further evaluate the performance of the phantom in a stimulative test bench as well as in real hardware measurements. In addition, the phantom could be enhanced by a dynamic time- and frequency-behavior.

References

- [1] Steffen Leonhardt and Burkhard Lachmann. Electrical impedance tomography: The holy grail of ventilation and perfusion monitoring? *Intensive Care Medicine*, 38(12):1917–1929, 2012.
- [2] D. C. Thomas, J. N. Siddall-Allum, I. A. Sutherland, and R. W. Beard. Correction of the non-uniform spatial sensitivity of electrical impedance tomography images. *Physiological Measurement*, 15(2A), 1994.
- [3] Vidya Sarode, Priya M Chimurkar, and Alice N Cheeran. Electrical Impedance Tomography using EIDORS in a Closed Phantom. *International Journal of Computer Applications*, 48(19):975–888, 2012.
- [4] Kenneth S. Cole and Robert H. Cole. Dispersion and Absorption in Dielectrics I. Alternating Current Characteristics. *The Journal of Chemical Physics*, 9(4):341–351, 1941.
- [5] Bartłomiej Grychtol, Beat Müller, and Andy Adler. 3D EIT image reconstruction with GREIT. *Physiological Measurement*, 37(6):785–800, 2016.
- [6] Michael J. Ackerman. The visible human project. *Proceedings of the IEEE*, 86(3):504–511, 1998.
- [7] Andy Adler and William R B Lionheart. Uses and abuses of EIDORS: an extensible software base for EIT. *Physiological Measurement*, 27(5):S25–S42, 2006.
- [8] D. Andreuccetti, R. Fossi, and C. Petrucci. An Internet resource for the calculation of the dielectric properties of body tissues in the frequency range 10 Hz - 100 GHz, 1997.
- [9] Camelia Gabriel. Compilation of the Dielectric Properties of Body Tissues at RF and Microwave Frequencies. *Environmental Health*, AFOSR-TR96(June):271, 1993.
- [10] Donald W. Marquardt. An Algorithm for Least-Squares Estimation of Nonlinear Parameters. *Journal of the Society for Industrial and Applied Mathematics*, 11(2):431–441, 1963.
- [11] Hervé Gagnon, Martin Cousineau, Andy Adler, and Alzbeta E. Hartinger. A resistive mesh phantom for assessing the performance of EIT systems. *IEEE Transactions on Biomedical Engineering*, 57(9):2257–2266, 2010.